Presumed PDF modeling of early flame propagation in moderate to intense turbulence environments

Christina Carmen [1] and Douglas A. Feikema [2, 3]

[1] Department of Mechanical and Aerospace Engineering
The University of Alabama in Huntsville
Huntsville, Alabama 35899, USA

[2] NASA Glenn Research Center
Microgravity Science Division
Microgravity Combustion Science, M.S. 77–5
Cleveland, Ohio 44135
Ph.: 216–433–5707
E-mail: douglas.feikema@grc.nasa.gov

[3] Corresponding Author

Physics and Astronomy Classification Scheme (PACS):

02.50 Ng	Distribution theory and Monte Carlo Studies
02.70 Uu	Applications of Monte Carlo methods
47.27.Eq	Turbulence Simulation and Modeling
47.27.Gs	Isotropic turbulence; homogeneous turbulence
47.70 Fw	Chemically reactive flows
52.80 Mg	Arcs; Sparks
82.33 Vx	Reactions in flames, combustion, and explosions

Abstract

The present paper describes the results obtained from a one-dimensional time dependent numerical technique that simulates early flame propagation in a moderate to intense turbulent environment. Attention is focused on the development of a spark-ignited, premixed, lean methane/air mixture with the unsteady spherical flame propagating in homogeneous and

isotropic turbulence. A Monte-Carlo particle tracking method, based upon the method of fractional steps, is utilized to simulate the phenomena represented by a probability density function (PDF) transport equation. Gaussian distributions of fluctuating velocity and fuel concentration are prescribed. Attention is focused on three primary parameters that influence the initial flame kernel growth: the detailed ignition system characteristics, the mixture composition, and the nature of the flow field. The computational results of moderate and intense isotropic turbulence suggests that flames within the distributed reaction zone are not as vulnerable, as traditionally believed, to the adverse effects of increased turbulence intensity. It is also shown that the magnitude of the flame front thickness significantly impacts the turbulent consumption flame speed. Flame conditions studied have fuel equivalence ratio's in the range $\phi = 0.6$ to 0.9 at standard temperature and pressure.

Nomenclature

Symbol	Definition
B	pre-exponential factor
B	reduced pre-exponential factor
C	concentration
$\overline{c_F}$	normalized mean fuel concentration, $\frac{Y_F}{Y_{Fst}}$
c'_F	root mean square (rms) fluctuation of normalized fuel concentration
C_{l_T}	coefficient of the integral length scale of turbulence
D/Dt	total or substantial derivative of
Da	Damköhler number
Da_T	turbulent Damköhler number
E_A	activation energy (Joule/mole)
E_{ign}	actual energy deposited into gas by ignition source spark energy
$E_{ign\text{-}min}$	minimum ignition energy
E_{sp}	electrical energy in the capacitance spark
k	turbulent kinetic energy
K	flame stretch
Ka	Karlovitz number

Ka'	Karlovitz flame stretch factor
Ka_∞	Karlovitz number for unstretched laminar flame conditions
l_T	integral length scale of turbulence
L_{sp}	distance between spark electrodes
Ma	Markstein number
n	total number of particles in a cell
N_{pc}	number of particles per cell
P	pressure, Joint Probability density distribution function
r	radial coordinate
R_u	Universal Gas Constant $\left(\frac{J}{mole \cdot K}\right)$
Re	Reynolds number
Re_T	turbulent Reynolds number based upon integral length scale
$R_L(t)$	time dependent radius of laminar flame ball
$R'_L(t)$	time dependent rate of increase of radius of laminar flame ball
$R_T(t)$	time dependent radius of turbulent flame ball
$R'_T(t)$	time dependent rate of increase of radius of turbulent flame ball
S^a	absolute flame speed
S^c	consumption flame speed
S^d	displacement flame speed
$S_d(0)$	displacement speed on the unburned gas side
$Sign$	initial energy deposited by spark
S_L	laminar burning velocity
$S_{L\infty}$	planar unstretched laminar burning velocity
S_L^a	laminar absolute speed
S_L^c	laminar consumption speed
S_L^d	laminar displacement speed
S_T	turbulent burning velocity
S_T^a	turbulent absolute speed
S_T^c	turbulent consumption speed
S_T^d	turbulent displacement speed
t	time
t_{chem}	chemical time
t_{sp}	duration of spark
t_T	turbulence time
t_η	Kolmogorov time
T	temperature
$\overline{\overline{T}}$	Favre averaged temperature
T_o	initial temperature
T_f	adiabatic flame temperature

T_A	activation temperature
u_i	velocity
u'	root mean square (rms) fluctuating turbulent velocity
U	mean gas velocity
$\bar{u}$	mean velocity
Y_α	species mass fraction
Y_F	fuel mass fraction
Y_{Fst}	stoichiometric fuel mass fraction
Y_p	product mass fraction
W	molecular weight
$x(t)$	position of particle j at time t

Greek	Definition
α	specie
α_R	reduced heat release factor
β_R	reduced activation temperature
δ_L	laminar flame thickness
δ_T	turbulent flame brush thickness
$\delta(\psi-\phi)$	dirac function
Δr	cell size in radial direction
Δt	time step
ΔR	distance traveled by fluid particle in on time step Δt
ε	rate of turbulent energy dissipation
η	Kolmogorov length scale
η_{sp}	spark efficiency
λ	Taylor microscale of turbulence
μ	dynamic viscosity
ν	kinematic viscosity
Ω	mixing frequency
Γ	
$\psi^{(j)}$	reactive scalar vector for particle j
ρ	density
ρ_b	burned gas density
ρ_u	unburned gas density
ϕ	fuel equivalence ratio
Θ	reduced temperature
$\dot{\omega}_\alpha$	mass rate of addition per unit mass of species α due to reaction
$\dot{\omega}_F$	local fuel reaction rate-rate at which the reactants are consumed by the chemical reaction

Subscripts	Definition
b	burned
F	fuel
i	particle i, coordinate direction
L	Laminar
sp	spark
st	stoichiometric
t	turbulent
o	initial

Superscripts	Definition
a	absolute
b	modified
c	consumption
d	displacement
j	particle counting
‘	root mean square fluctuating parameter, first derivative with respect to time
“	flux, per unit area

1. Introduction

This paper is concerned with the numerical computation of early flame propagation for a spark-ignited, premixed methane/air gas in a moderate to intense turbulent environment. Real combustion processes occurring in such devices as internal combustion engines, rockets, natural gas burners, industrial power plants and gas-turbine engines nearly always occur within a flow field of moderate to intense turbulence. Several developments and modifications to the original algorithm have been implemented including a revised chemical reaction scheme and the evaluation and calculation of various turbulent flame properties. Several complex phenomena and topics are considered including spark ignition, turbulence, reacting flows and statistical methods. Attention is focused on the early stage of the flame front development as this stage is greatly influenced by turbulence and, thus, significantly influences overall engine performance. However, the aerodynamics of the flow, both convection and turbulence, is not the only

influence on the flame. As a result, vital influences such as the composition of the mixture and the characteristics of the ignition system such as energy delivered, spark plug geometry, and spark duration are also taken into account.

Although numerous experimental and numerical studies on turbulent combustion have been developed, a common approach has not emerged due to the complexity of the physical and chemical phenomena occurring in turbulent flames. Recent reports [19, 20] have established the fact that a great deal of discrepancy still exists concerning how turbulent flame speeds are defined. The present work attempts to clarify these discrepancies by incorporating the absolute, displacement and consumption flame speeds as defined by Poinsot and Veynante [20]. Computing and accounting for the flame thickness and stretch and their effects upon the value of the flame speed will also be evaluated. Turbulent cases focus on the effect of varying turbulence intensity upon such characteristics as flame position, turbulent flame speed, and turbulent flame regimes. Attention is focused upon the distributed reaction zone where moderate to intense turbulence conditions exist. Traditionally, the theoretical foundation of the distributed reaction zone has been evaluated differently than the wrinkled flame regime and the corrugated flame regime. Recently within the turbulent combustion community, particularly in experimental research [7], there have been conclusions drawn that the distributed reaction zone is not as vulnerable an environment as traditionally believed and that a viable flame front can be sustained without the imminent threat of flame quenching.

Computations involving turbulent conditions focus on the effect of parameters such as the ratio of the root mean square (rms) turbulent velocity to the laminar burning velocity, u'/S_L, and the turbulent Reynolds number, Re_T, on various flame properties. Parameters such as the

ignition energy required and the quenching distance are verified. The described method produces results similar, if not identical, to those produced experimentally and numerically.

2. Formulation of the problem

In the present study chemical parameters have been set to simulate various premixed methane/air combustible mixtures at normal temperature and pressure (298.15 *K* and 1 *atm)*. Lean methane/air flames are investigated with fuel equivalence ratios ranging from 0.6 to 0.9. The premixed gaseous mixture is initially quiescent in a non-decaying turbulent environment with the turbulence intensity varying from 0.5 *m/s* to 2 *m/s*. The mixture is assumed to be a perfect gas and one-step Arrhenius chemistry is utilized. A one-dimensional, spherically symmetric geometric model is considered and is shown schematically in Figure 1. The calculations simulate ignition of the premixed gaseous mixture by a spark ignition device. If the appropriate thermal requirements are met a spherical flame propagates radially outward from the point of ignition. The present analysis focuses on the flame front and flow conditions within milliseconds after successful ignition. During this time the combustion chamber pressure does not significantly change [16]. As a result, a constant pressure environment at 1 *atm* is assumed.

All results and calculations are made with respect to the center of the initial spark. The random motion of the center of the flame ball is not taken into account. Thus, results, such as the change in flame radial position, are calculated relative to the center of the initial spark.

Finite difference solutions of the Navier-Stokes equations are often not practical, mainly because of the large dimensions of the PDF's. Thus, in the present study the approach chosen for obtaining a solution is an equation for the joint PDF of chemical and thermodynamic properties in turbulent reactive flows. The transport equation for the joint PDF is modeled and solved by a

Monte-Carlo method that simulates the representative terms in the PDF transport equation by the method of fractional steps. A Gaussian distribution for the normalized fuel concentration and fluctuating velocity is presumed. In the Monte-Carlo particle tracking method the fluid particles advance in space and are taken through representative collisions and chemical reactions. Each particle's position coordinates, velocity components, and internal states are stored and modified with time.

2.1 Probability Density Function transport equation

Starting from the conservation equations, with the assumption of low mach number and high Reynolds number, the properties at any point within the flame can be determined from a PDF transport equation [21]. Pope [22] proposed the use of a transport equation for the joint PDF of velocity, viscous dissipation, and reactive scalars. However, this equation does not include scalar gradients and therefore contains no information about the mixing time scale. Dopazo [9] therefore advocated the use of a transport equation for the joint statistics of velocity, velocity gradient, reactive scalars, and their gradients. In this equation, in addition to convection and chemical reaction being closed, so also is the term that describes the straining and rotation of scalar gradients, a mechanism that is believed to be essential in turbulent reacting flows. The closure problem is, however, shifted to the mixing of scalar gradients. This formulation has not yet been applied to flows with combustion [17].

In the current analysis the transport equation for the joint PDF of velocity and reactive scalars is considered [22]. The reactive scalars, such as the mass fraction of reacting species (the progress variable), can be represented by the vector $\tilde{\psi}$ The PDF transport equation provides a description of the transport of the PDF $\overline{\overline{p}}(\psi)$ in position and composition (species) spaces. The

main interest of the PDF transport equation is that the chemical reaction term depends only on chemical variables and does not require any modeling. Thus, the effect of chemical reaction on transport in composition space appears in closed form.

The transport equation for the density-weighted joint PDF is:

$$\underbrace{\overline{\rho}\frac{\overline{D\tilde{p}(\psi)}}{Dt}}_{MeanFlowConvection} + \underbrace{\frac{\partial\overline{\rho u_i''\tilde{p}'(\psi)}}{\partial x_i}}_{TurbulentTransport} = - \underbrace{\frac{\partial\overline{\rho}\tilde{p}(\psi)\dot{\omega}_\alpha(\psi)}{\partial\psi_\alpha}}_{Chemical\,Reaction} - \underbrace{\frac{\partial}{\partial\psi_\alpha}\overline{p'(\psi)\frac{\partial}{\partial x_i}\Gamma\frac{\partial\phi_\alpha}{\partial x_i}}}_{MolecularMixing} \qquad (1)$$

where $p'(\psi)$ is written for $\delta(\psi-\phi)$. The derivation and in-depth explanation of this equation is provided by Pope [21]. The terms on the left-hand side of equation (1) represent convection by the mean flow and by turbulence; they account for the transport of $\tilde{p}(\psi)$ in physical (i.e. flow field) space. The terms on the right hand side account for the transport of $\tilde{p}(\psi)$ in composition space due to chemical reaction and mixing. For chemically reacting flows it is of particular interest that the chemical source terms can be treated exactly for arbitrarily complex chemical kinetics. It has often been argued that in this respect the transported PDF formulation has a considerable advantage compared to other formulations. For chemically reacting flows the last term in (1), which represents the transport in reactive scalar (composition) space by molecular fluxes, is the most difficult to model. This term represents molecular or micro-scale mixing.

Although the velocity-composition joint PDF is a function of many independent variables, its evolution equation can be solved by a Monte-Carlo method. Virtually all numerical implementations of PDF methods for turbulent reacting flows utilize Monte-Carlo simulation techniques [21, 17] in which the joint PDF is represented indirectly by a large number of

particles. The Monte-Carlo method tracks the individual particles through each of the phenomena represented in equation (1) by the method of fractional steps.

2.2 The Monte-Carlo particle tracking method

The Monte-Carlo solution strategy utilized is based on the concepts presented by Pope [22]. Monte-Carlo methods employ a large number of particles that can be considered as different realizations of the turbulent reactive flow problem under investigation. In the Lagrangian algorithm [21] the particles are not bound to grid nodes. Instead, each particle has its own position and moves through the computational domain with its own instantaneous velocity. Thus, the state of the particle is described by its position and velocity, and by the values of the reactive scalar that its represents as a function of time. The simplest method to estimate local means is to compute cell averages. Computationally, the radial direction is composed of a prescribed number of "cells" each with a specified radial length, Δr. Each cell is initially assigned a certain number of fluid particles with each particle having a prescribed velocity, fuel concentration, and temperature. For the results reported herein, each cell initially contains 1000 particles. As time marches forward the number of particles within each cell changes as the flame propagates radially outward.

In the Lagrangian simulation, typically the method of fractional steps [21, 17] is used. This method is based on the observation that the various terms describing the time evolution of the PDF in equation (1) are additive. Therefore the processes in physical, velocity, and reactive scalar space may be treated sequentially rather than simultaneously. For one-dimensional calculations the Lagrangian motion of particle j is given by

$$\frac{dx^{(j)}}{dt} = \quad u^{(j)}(x), \tag{2}$$

or

$$x^{(j)}(t+\Delta t) = x^{(j)}(t) + u^{(j)}\Delta t \tag{3}$$

where the velocity $u^{(j)}$ describes the motion of particle j. According to the theory of stochastic differential equations the evolution of the spatial distribution of particles is represented by the first term on the left hand side of the transport equation for the density weighted joint PDF (equation 1). Similarly, the change of the composition value ψ_i of the reactive scalars of the Lagrangian particle j, is given by

$$\rho^{(j)} \frac{d\psi^{(j)}}{dt} = \omega^{(j)}, \tag{4}$$

or

$$\psi_i^{(j)}(t+\Delta t) = \psi_i^{(j)}(t) + \frac{\dot{\omega}_i^{(j)}}{\rho^{(j)}}\Delta t\,. \tag{5}$$

Equation (5) represents the first term on the right hand side of the PDF transport equation. This illustrates how the solution of only time-dependent Lagrangian equations for particles simulates the solution of the transported PDF equation.

The main drawback of Monte-Carlo methods is that they suffer from a statistical error that decreases only slowly with the number of particles N_{pc} per cell [17]. The error is proportional to $1/\sqrt{N_{pc}}$. For an acceptable numerical accuracy far more than a hundred particles must be present in each cell. For industrial CFD problems, which require large

numerical grids consisting of typically several hundred thousand grid cells, this leads to very large numbers of particles. Xu and Pope [26] have quantified the different errors that occur in Monte-Carlo methods for turbulent reactive flows. Monte-Carlo techniques are known to be sensitive to the number of cells, the number of particles, the mixing model, and initial conditions (i.e. spark shape and duration).

3. Numerical procedure

The numerical procedure is a fluid particle tracking method that approximates equation (1). The convective transport of the particle by the mean flow and by turbulence is accounted for in space and in time by the terms on the left-hand side of the transport equation. The chemical and thermal composition of each particle changes due to molecular mixing and chemical reaction as represented by the terms on the right-hand side of the transport equation.

3.1 Input parameters

Due to the large number of parameters involved in a spark ignited, turbulent flame analysis adjustment of parameters can enhance numerical results. It is important to note that in the current modeling, no ad-hoc adjustment of any parameter has been made. All parameters have their correct values throughout the analysis and were obtained from experimental measurement, theory or from the results of a thermodynamic analysis. When comparison is made to the work of other researchers, all ignition, mixture and flow conditions reported by the researcher are implemented in the present work.

The following input values are required: time step, Δt, cell width, Δr, turbulent kinetic energy, k, dissipation of turbulent kinetic energy, ε, normalized mean fuel concentration, $\overline{c_F}$,

root-mean-square fluctuation of fuel concentration, c'_F, chemical time, t_{chem}, coefficient of ignition, S_{ign}, pressure, P, spark duration, t_{sp}, spark gap, L_{sp}, activation temperature, T_A, adiabatic flame temperature, T_f, initial reactant temperature, T_o, pre-exponential factor, B, and the laminar flame speed, S_L.

A chemical equilibrium calculation with dissociation using CEC Gordon and McBride code [11] is utilized to determine the adiabatic flame temperature. The adiabatic flame temperature is required in the calculation of the reduced temperature, θ, and in the Arrhenius reaction rate model. Table 1 provides values of the adiabatic flame temperature predicted by the algorithm.

Table 1 Adiabatic flame temperatures for Methane/Air as computed using CEC [11] for lean mixtures as a function of ϕ

Methane/Air Fuel Equivalence Ratio, ϕ	**Adiabatic Flame Temperature, T_f (K)**
0.6	1554.76
0.7	1718.25
0.8	1871.33
0.9	2011.50

3.2 Chemical time

The chemical time is defined as $t_{chem} = \nu/S_L^2$ where ν is the kinematic viscosity. The chemical time is required in the calculation of the turbulent Damköhler number, Da_T. Various values of ν and S_L are reported in combustion literature. Kinematic viscosity values of 15.5 x 10^{-6} m^2/s, 15.7 x 10^{-6} m^2/s and 16.0 x 10^{-6} m^2/s for a methane/air mixture are reported by Gülder [12]. The laminar burning velocity is dependent upon the fuel equivalence ratio, ϕ. Values of S_L can vary

based upon the various formulations including numerical, experimental and asymptotic methods [19]. Therefore, the value of t_{chem} can vary significantly depending upon the values of ν and S_L utilized. Because the values of t_{chem} and Da_T are very sensitive to the laminar burning velocity, S_L, reliable S_L data for lean premixed methane/air flames is important in the present study. This is especially critical for $\phi < 0.7$ where S_L becomes very small (≈ 0.1 *m/s*) and the scatter in theoretically calculated S_L data can be as high as 200 percent [6]. Throughout the present work the kinematic viscosity is assigned a value of 15.7 x 10^{-6} m^2/s as reported by Gülder [12] for a lean methane/air mixture. The asymptotically based values of S_L provided by Poinsot and Veynante [20] are implemented in the present study. Table 2 provides the calculated values of t_{chem} and the values of S_L utilized in all Monte-Carlo simulations.

Table 2 Chemical time and laminar burning velocity values utilized in the Monte-Carlo method.

Methane/Air Fuel Equivalence Ratio, ϕ	**Laminar Burning Velocity S_L (*m/s*)**	**Chemical Time t_{chem} (*ms*)**
0.6	0.13	0.929
0.7	0.21	0.356
0.8	0.28	0.200
0.9	0.36	0.121

3.3 Activation temperature

Poinsot and Veynante [20] present the parameters used in flame speed computations for a methane/air flame modeled by a single step reaction. An activation energy of 83,600 *J/mole* was utilized as it is in the present work. The activation temperature, $T_A = E_A/R_u$, utilized is 10,055 *K*.

3.4 *Turbulence parameters*

The constants calculated in the algorithm include the integral length scale of turbulence, l_T, turbulence time, t_T, and the turbulent Reynolds number, Re_T, which are defined as follows:

$$l_T = \frac{u'^3}{\varepsilon} = C_{l_T}\left[\frac{\kappa^{1.5}}{\varepsilon}\right] \tag{6}$$

$$t_T = \frac{l_T}{u'} \tag{7}$$

$$Re_T = \frac{u' l_T}{\nu} \tag{8}$$

The above definitions for turbulence time and turbulent Reynolds number are generally agreed upon. However, the coefficient C_{l_T} of the integral length scale of turbulence assumes various values throughout literature [1, 18, 23] depending on the exact method of formulation. Isotropic turbulence is assumed in the present work. Therefore, $k = (3/2)u'^2$ or $u' = \sqrt{(2/3)k}$ and the integral length scale of turbulence and the turbulence time are defined as:

$$l_T = \frac{u'^3}{\varepsilon} = \left(\frac{2}{3}\right)^{1.5}\frac{k^{1.5}}{\varepsilon} \tag{9}$$

$$t_T = \frac{l_T}{u'} = \frac{\left(\frac{2}{3}\right)^{1.5}\frac{k^{1.5}}{\varepsilon}}{\sqrt{\frac{2}{3}k}} = \frac{2}{3}\frac{k}{\varepsilon} \tag{10}$$

The turbulence is non-decaying. Thus, the turbulence kinetic energy and the dissipation of turbulent kinetic energy are constant throughout a computation. This assumption does not introduce large errors since the computational time is typically 5 ms and the turbulence times are shown in Table 3 range from 0.121 ms to 0.929 ms.

3.5 *Gaussian distributions*

The initial fuel concentration and fluctuating velocity are prescribed a Gaussian distribution. After the initial Gaussian distribution is calculated for the fuel concentration, the subsequent concentration distribution proceeds randomly in time changing only due to mixing and reaction. The Gaussian distribution for the fluctuating velocities is updated at every interval of the turbulence time.

The fluctuating velocities have a spatial correlation that is a function of the turbulent length scale. The correlation follows a simple zero order Frankiel decreasing exponential calculation. The random deviates of the Gaussian distribution are calculated using the Box Müller method. The normal deviates have a zero mean and unit variance. Initially each particle is assigned a fluctuating velocity and a fuel concentration value. Both the mean and root mean square fluctuations of velocity and fuel concentration are specified. Initially, since the premixed gas is at rest, the mean velocity is zero.

3.6 Particle diffusion

During each time step the particles in each cell move a certain distance based upon the instantaneous velocity and time step, Δt. The instantaneous velocity, u, is the sum of the mean

velocity, U, and the fluctuating velocity, u'. Thus, during each time step, each cell either loses or gains particles. For example, in the one-dimensional analysis the distance, ΔR, traveled by a fluid particle is defined as follows:

$$\Delta R = (U + u') \Delta t \tag{11}$$

Initially, the mixture is stationary and $U(0) = 0$. These calculations provide the simulation of the propagation of the flame. As the flame propagates outward from the point of ignition, the density of the particles behind the wave decreases. Simulation of wave propagation is imperative since successful ignition of most combustion systems depends not only on the ignition of the fuel-oxidizer mixture, but also on the ability of the spark ignited flame kernel to propagate from the point of ignition. In many combustion systems it is in fact flame propagation rather than ignitability which determines the flammability limits.

3.7 Micro-scale mixing

These calculations follow the model of Curl [8]. More elaborate mixing models exist; however, at the expense of increased computational requirements and complexity. Curl's model is a coalescence and redispersion model of the concentration and temperature. A random number generator randomly selects colliding particles. For example, when two particles of concentration C_1 and C_2 mix one particle is formed with a concentration $C = C_1 + C_2$. Upon redispersion there are two particles each with a concentration $C_1' = C_2' = \frac{1}{2}(C_1 + C_2)$. During small scale mixing not all of the particles will collide. The number of particles that mix is determined by the mixing frequency. The mixing frequency, Ω, is the percentage of particles mixed per each time step.

The following empirically derived mixing frequency utilized by Borghi and Mantel [4] is employed in the present analysis:

$$\Omega = 0.625 \left[\frac{\Delta t}{t_T} \right] \tag{12}$$

3.8 Chemical reaction

The chemical reaction is represented by a single-step Arrhenius chemistry mechanism,

$$\text{R (reactants)} \neg \quad \text{P (products)} \tag{13}$$

and the reaction rate $\dot{\omega}_R$ is expressed as,

$$\dot{\omega}_R = B \rho \ \overline{c_F} \exp\left(\frac{-T_A}{T} \right) \tag{14}$$

where B is the pre-exponential factor. This expression is more conveniently cast in the form following [25, 18, 20]:

$$\dot{\omega}_R = B \rho \, \overline{c_F} \exp\left(\frac{-\beta_R (1-\Theta)}{1-\alpha_R (1-\Theta)} \right) \tag{15}$$

Θ is the reduced temperature,

$$\Theta = \frac{T - T_o}{T_f - T_o}, \tag{16}$$

where T_o is the unburned fresh gas temperature and T_f is the adiabatic flame temperature for unity Lewis number. The activation temperature is T_A, and the coefficients B, α_R, and β_R are, respectively, the reduced pre-exponential factor, the reduced heat release factor and the reduced activation temperature, defined as follows:

$$B = \mathrm{B} \exp\left[\frac{-\beta_R}{\alpha_R}\right] \tag{17}$$

$$\alpha_R = \frac{T_f - T_o}{T_f} \tag{18}$$

$$\beta_R = \alpha_R \left[\frac{T_A}{T_f}\right] \tag{19}$$

The two parameters α_R and β_R measure the heat released by the flame and the activation temperature respectively. The values of α_R and β_R used in the present work for $T_A = 10{,}055K$ are presented in Table 3.

Table 3 Values of α_R and β_R used in the Reaction Rate Model

Methane/Air Fuel Equivalence Ratio, ϕ	**Adiabatic Flame Temperature, T_f (K)**	α_R	β_R
0.6	1554.76	0.8083	5.23
0.7	1718.25	0.8266	4.84
0.8	1871.33	0.8407	4.52
0.9	2011.50	0.8519	4.26

3.9 Spark ignition

The spark energy decreases linearly in time and decreases parabolically with distance from the point of ignition [5, 6]. The spark does not produce any more energy after the specified ignition time, t_{sp}, nor does it deposit energy at a distance exceeding the spark gap length, L_{sp}. The total energy deposited by the spark in the spherically symmetric environment is [6]:

$$E_{ign} = \frac{\pi^2}{15} \eta_{sp} S_{ign} t_{sp} L_{sp}^3. \tag{20}$$

The present ignition model contains a spark efficiency, η_{sp}, to account for losses in actual spark ignition systems. In actual spark ignition systems much of the electrical energy is expended in radiative losses, shock wave formation, and convective and conductive heat losses to the electrodes and flanges [10]. Flanges connected to the electrodes are often used in actual spark ignition systems. Zeldovich [27] reports the spark efficiency for mixtures varies from 2-16%. The spark efficiency is the ratio of external input energy required in order to heat a spherical

volume of gas to its adiabatic flame temperature to the total energy in a capacitance spark. Therefore, the energy required to ignite a mixture is equal to 2-16% of the electrical energy in the spark due to the losses described by Glassman [10]. In the present computer model a spark efficiency of 10% is employed in order to computationally account for and model actual losses associated with real world spark electrodes.

3.10 Average cell temperature and density

During each time step the Favre averaged temperature of each cell is calculated as follows:

$$\overline{\overline{T}} = \frac{\sum_{i=1}^{n} \rho_i T_i}{\sum_{i=1}^{n} \rho_i} \tag{21}$$

where n is the number of particles in the cell during the current time step. Upon substitution of the ideal gas law in equation (21), the average temperature can be expressed as follows:

$$\overline{\overline{T}} = \frac{\sum_{i=1}^{n} \frac{P}{R}}{\sum_{i=1}^{n} \frac{P}{RT_i}} \tag{22}$$

or

$$\overline{\overline{T}} = \frac{n}{\sum_{i=1}^{n} \frac{1}{T_i}} \tag{23}$$

The Favre averaged density of each cell is calculated using the ideal gas law at constant pressure, P, and the computed Favre average temperature, $\overline{\overline{T}}$, of each cell:

$$\overline{\overline{\rho}} = \frac{P}{\frac{R_u}{W}\overline{\overline{T}}} \tag{24}$$

where W is the mean molecular weight of the mixture given by:

$$\frac{1}{W} = \sum_{\alpha=1}^{N} \frac{Y_\alpha}{W_\alpha} . \tag{25}$$

Initially, for the unburned fresh gas methane/air mixture, W = 29 kg/kgmol. Therefore, for the unburned gas mixture, equation (24) can be written as:

$$\overline{\overline{\rho}} = \frac{P}{287(J/kg-K)\overline{\overline{T}}} \tag{26}$$

The reduced, non-dimensional temperature of each cell is calculated using equation (16).

3.11 Average cell velocity

During each time step the discretized equation of continuity is solved for the average velocity of each cell:

$$\frac{\overline{\Delta\rho}}{\Delta t} + \frac{1}{r^2}\frac{\Delta(\overline{\rho U} r^2)}{\Delta r} = 0 \qquad (27)$$

Initially, the gas mean velocity is zero or $U\,(t = 0) = 0$. $\overline{\rho U}$ is the ensemble or time averaged, density weighted velocity at a fixed radial location.

3.12 *Flame front position*

The numerically simulated results are analyzed similarly to other numerical and experimental measurements [2, 23] that base the flame position on the point where the normalized fuel concentration, or temperature, is the average of the hot and cold boundaries.

3.13 Post-processing

The Gordon and McBride CEC code [10] is also utilized to verify the burned to unburned gas density ratio used in the calculation of the turbulent burning velocity. Aung et al. [2] similarly utilized the CEC algorithm to determine the density ratio. It should be noted, however, that this approach represents a convention that ignores preferential diffusion effects. These effects modify the local mixture ratio and thermal energy transport for stretched flames, and thus the local density ratio of the flames. However, as noted by Aung et al. [2] this convention is convenient because a single density ratio is used to relate flame speeds (i.e. absolute speeds) and burning velocities or displacement speeds for all levels of flame stretch. This avoids the current uncertainties about the effects of stretch on the jump conditions across flames for particular conditions in the unburned gas mixture. Numerical simulations provide a means of estimating density ratio variations but there are still uncertainties concerning the reliability of the

calculations. Furthermore, Aung et al. [2] estimate that variations of flame properties due to variations of density ratios with stretch do not exceed 11%. This variation is significantly less for fuel lean conditions where Markstein numbers, and thus the effects of stretch, are small. This contrasts fuel-rich conditions where Markstein numbers, the effects of stretch, and thus, the variation of properties due to density ratio variations are large.

Table 4 Burned to Unburned gas density ratio computed using CEC code [10] as a function of ϕ

Methane/Air Fuel Equivalence Ratio, ϕ	**Density Ratio, ρ_b/ρ_u**
0.6	0.1859
0.7	0.1675
0.8	0.1534
0.9	0.1420

4. Preliminary results

4.1 Monte-Carlo sensitivity

As previously mentioned, Monte-Carlo methods are sensitive to input parameters such as the spark ignition characteristics and the number of particles initially assigned per cell. A 20 percent difference in calculated flame property values can result when 100 particles per cell are used instead of 1000 particles per cell. A plot of the flame front radial position versus time from

spark onset is provided in Figure 2. The results are based upon the initial assignment of 100 particles per cell. Figure 2 provides the results of 10 identical turbulent flame simulations using the present Monte-Carlo method. The average curve of these ten simulations is also presented. Figure 3 is based on simulations identical to Figure 2 except that 1000 particles were initially assigned to each cell. It is obvious that utilizing 1000 particles per cell generates less scatter in the results. The results of individual executions using 1000 particles per cell are much more reliable than individual executions generated using 100 particles per cell. Also, the average flame radial position generated utilizing 1000 particles travels faster than the flame generated using 100 particles per cell. At approximately 8 *ms* the flame position in Figure 2 is approximately located at 4.3 *mm*. In Figure 3, at 8 *ms*, the flame radial position is located at approximately 5.0 *mm*. Thus, there exists approximately a 16 percent difference in flame radial position between 100 particles per cell versus 1000 particles per cell. In the present work 1000 particles are initially assigned per cell. All results provided are based on the averages of 10 individual simulations in order to reduce error.

4.2 Quenching distance

The quenching distance is the critical distance between spark electrodes that will allow an inflamed spark kernel to grow unaided. Experiments conducted by Lewis and Von Elbe [15] utilized flanges connected to the tips of the electrodes. These flanges were made from an electric nonconductor such as glass so that the sparks remained centered between the electrodes. Calculations for ϕ = 0.9 (methane/air), with u' = 0.0 m/s and c'_F = 0.0, using the current numerical model show the quenching distance to be 2 *mm*. This matches exactly the experimentally determined quenching distance of Lewis and Von Elbe [15] for the same mixture.

The quenching distance is determined by varying the spark electrode gap distance, L_{sp}, while keeping all other conditions and variables constant until the point of ignition is reached. For values of L_{sp} up to 1.9 *mm* the flame does not ignite. As L_{sp} is increases from 1.9 *mm* to 2.0 *mm* the flame ignites and propagates outward from the center of the initial spark.

4.3 Minimum ignition energy

The minimum ignition energy is the least amount of energy required from the spark to create a spark kernel at the quenching distance. The current model predicts a required minimum ignition energy, $S_{ign\text{-}min}$, of 0.25 to 0.3 *mJ* for L_{sp} = 2.0 *mm* and ϕ = 0.9 at 1 *atm*. This value was determined in the same manner as was the quenching distance. The initial energy deposited by the spark, S_{ign}, was increased, while all other conditions and variables remained constant, until ignition and flame propagation was observed. This compares very well to the experimental data of Lewis and Von Elbe [15] who report a required minimum ignition energy of 0.28 *mJ* to ignite an equivalent mixture of methane/air for L_{sp} = 2.0 *mm* and ϕ = 0.9 at 1 *atm*. Blanc et al. [3] also report a minimum ignition energy of 0.28 *mJ* for the same mixture.

5. Turbulent flame results

The purpose of the present results is to demonstrate that the current model is a viable predictor of the effect of the mixture composition, the aerodynamics of the flow and the characteristics of the ignition system upon early flame propagation in a moderate to intense turbulence environment.

The turbulent flame speed and burning velocity is not only a function of the fuel-oxidizer mixture ratio but also of the flow characteristics and the ignition source configuration. Therefore, there can exist great difficulty in correlating both experimental and numerical data of

various investigators. When comparing the present results to various experimental and numerical results of other researchers, every attempt has been made to simulate the conditions of the referenced work.

The exact formulation of all Monte-Carlo results with respect to the turbulent absolute, displacement and consumption speed will be established. When comparison is made to the flame speed results of other researchers and no definitive clarification was provided in regard to a kinematic or reaction based formulation, the turbulent flame speed is referred to as the turbulent burning velocity. However, displacement based formulations are most commonly reported in the literature even though not directly specified. When the flame thickness is neglected the displacement and consumption speeds are approximately identical. Evaluation of the turbulent flame regime criteria, the effect of turbulence intensity and predictions of various turbulent flame speeds calculated using the present Monte-Carlo code are presented and compared to the values of other researchers. Attention is focused on flames in the distributed reaction zone regime.

5.1 *Turbulent Flame Properties*

Flames with varying degrees of turbulence intensity are examined. The properties associated with these flames are shown in table 5. In each case the unburned gas temperature is 298 K, the activation temperature is 10,055 K, the pressure remains constant at 1 atm and the kinematic viscosity, ν, is 15.7 x 10^{-6} m^2/s [12]. Note the following notation utilized in Table 5: laminar displacement speed, S_L^d, laminar flame thickness, δ_L, modified laminar flame thickness, δ_L^b, Kolmogorov time, t_η, Karlovitz number, Ka, Karlovitz flame stretch factor, Ka', Kolmogorov length scale, η, Taylor microscale of the turbulence, λ.

5.2 *Turbulent Flame Regimes*

Classification of turbulent premixed flames continues to evolve after various regimes were originally defined over 60 years ago. The classification presently utilized follows the standard prescribed by the Borghi-Barrière diagram [7]. In this diagram the $Ka = 1$ boundary, commonly referred to as the Klimov-Williams criterion, separates the regimes of wrinkled laminar flames from flames with thicker distributed reaction zones. Currently, among combustion researchers, there is much interest in verifying experimentally the changes in flame structures as predicted by the Klimov-Williams criterion [7]. This is due to the fact that many practical systems span the criterion boundary and theoretical treatments of the two flame regimes can be quite different. For values of $Ka > 1$ the flame is defined as being in the distributed reaction zone regime. Traditionally the distributed reaction zone regime has been viewed as incapable of sustaining a flame due to the fluctuations in temperature, concentration and velocity. Recently however, numerical and theoretical data seems to suggest that flamelets are more resilient to penetration by small eddies than is prescribed by the Klimov-Williams criterion.

Monte-Carlo results for various flames seems to support the latest views that the distributed reaction zone regime of $Ka > 1$ should be interpreted as the regime where the probability for small intense turbulence to penetrate the flame sheet is finite [7]. Based upon the Borghi-Barrière diagram most of the turbulent flames currently simulated are specified as occurring in the distributed reaction zone regime. Table 6 provides specific values of regime criteria as a function of the laminar flame thickness, δ_L, and a modified laminar flame thickness, δ_L^b. The modified laminar flame thickness is a function of the adiabatic and initial flame temperature and is a more precise estimate of the laminar flame thickness [20].

Table 6 Flame Regime criteria

Flame	$\frac{u'}{S_L}$	$\frac{l_T}{\delta_L}$	$\frac{l_T}{\delta_L^b}$	*Ka*	*Flame Regime*
F1	2.5	25	3.5	0.791	Corrugated
F2	2.5	52	7.3	1.40	Distributed
F3	2.5	48	6.7	1.53	Distributed
F4	2.5	50	6.9	1.57	Distributed
F5	2.5	52	7.2	1.64	Distributed
F6	2.5	54	7.4	1.69	Distributed
F7	2.5	55	7.6	1.75	Distributed
F8	2.5	57	7.9	1.80	Distributed
F13	2.5	69	9.5	2.17	Distributed

Depending upon which value of the laminar flame thickness is used, δ_L or δ_L^b, a large difference exists in the values of the ratio of the integral length scale to the laminar flame thickness. This difference is readily apparent in Figure 3 in which flames *F1*-*F8* and *F13* are assigned to their respective flame regimes based upon the criteria presented in Table 6.

5.3 Concentration, Density and Velocity Profiles

Time evolution of the normalized fuel concentration, density, and mean velocity of a typical case run represented by the parameters associated with flame *F1* are shown in Figures 5, 6, 7, and 8.

Figure 5 displays the time history of the normalized fuel concentration versus the flame radial distance. It is readily observed that the flame is propagating radially outward. The value of the fuel concentration drops to zero indicating complete combustion at the center. It is from the normalized concentration profiles that the flame radial position and absolute flame speed are calculated. The radial position of a flame front is taken where the normalized concentration is the equivalent of half of the initial normalized fuel concentration. This is a common convention used by various combustion researchers [23].

The gas density plotted against the radial distance for various times from spark onset for flame *F1* is shown in Figure 6. The ratio of the burned gas density to the unburned gas density, ρ_b/ρ_u, is approximately 0.1. The ratio predicted by the Gordon McBride CEC code [11] for ϕ = 0.8 is 0.1534. This value is common for most practical gaseous hydrocarbon flames in which the burned to unburned gas density ratio lies in the range 0.1 to 0.2 [1].

The mean gas velocity versus radial distance is shown in Figures 7 and 8. The large initial increase in the mean velocity obvious at 0.4 *ms* is a result of the initially rapid volume expansion created by the spark ignition energy. The spark ignition energy weakens due to an imposed linear decay in time and a parabolic decay in distance. The spark is ignited a duration of 1.5 *ms*. It can be observed in Figure 7 that between 0.4 and 1.6 *ms* the mean velocity decreases with the lowest maximum values occurring at 1.6 *ms*. After the 1.5 *ms* spark duration the velocity again increases.

Figure 7, in comparison to Figure 5 and Figure 6, shows that the highest radial gas velocities occur within the flame front. For example, it can be seen from Figure 6 that the maximum gas velocity at 2.8 *ms* occurs at approximately 3 *mm*. By comparison with Figure 5 and Figure 6 it is observed that this position lies between the burned and unburned regions of the

flame front. Thus, the maximum mean gas velocity occurs within the turbulent flame brush. It has been well established that in all flames there is a large increase in velocity as the gases enter the burned gas state [10]. Therefore, heat release itself can play a role in inducing turbulence. However, the effect of heat release upon turbulence properties is not considered in the present work as turbulence is assumed to be non-decaying.

5.4 Turbulent Flame Absolute Speed

The turbulent flame absolute speed, S_T^a, is also referred to as the flame propagation speed or, for turbulent spherical flames, the rate of increase of the turbulent flame ball radius $R_T'(\mathrm{t})$. Similar to the laminar cases, this speed can be obtained by calculating the slope of the time evolution of the flame radial position. Pope and Cheng [23] previously developed a Monte-Carlo numerical solution of the modeled equation for the joint PDF of the velocities and the reaction progress variable. Pope and Cheng [23] also present the turbulent flow experimental results generated by Hainsworth [14]. The experimental investigations generated turbulence by passing a premixed methane/air mixture through a turbulence-generating perforated plate producing a uniform mean flow of homogenous, isotropic turbulence. The mixture was ignited downstream of the plate forming a spherical flame kernel that expanded and was distorted by the turbulence. A comparison of the results of the present model with those of Hainsworth [14] and Pope and Cheng [23] is presented in Figure 8 which shows the time evolution of the flame front radial position. The turbulence intensity, u', is 1.93 *m/s* and ϕ = 0.8. Other properties of the Monte-Carlo simulated flame are provided in Table 5 for flame ***F13***. As seen in Figure 9 between 0 and approximately 2 seconds S_T is approximately equal to the laminar displacement speed, S_L^d. Between 2 and 5 seconds S_T increases above the laminar value. This observation is consistent

with previous observations of Anand and Pope [1] and Rutland et al. [24]. Excellent agreement exists between the present Monte-Carlo method, the experiments of Hainsworth [14] and the statistical calculations of Pope and Cheng [23]. The absolute flame speed calculated by the Monte-Carlo method is 3.8 *m/s*.

5.5 Turbulent Flame Displacement Speed

Similar to the laminar displacement speed the turbulent displacement speed, S_T^d, is defined as

$$S_T^d = \left(\frac{\rho_b}{\rho_u}\right) R_T'(t) = \left(\frac{\rho_b}{\rho_u}\right) S_T^a \tag{28}$$

where $R_T'(t)$ is the rate of increase of the turbulent flame ball radius, $R_T(t)$. $R_T'(t)$ is the turbulent flame propagation speed and is also referred to as the turbulent flame absolute speed, S_T^a. Recall, the results of the Gordon McBride CEC code [11] report a density ratio, ρ_b/ρ_u, of 0.1534 for ϕ = 0.8. Therefore, the present model predicts the turbulent displacement speed to be 0.58 *m/s*.

5.6 Turbulent Flame Consumption Speed

When the flame thickness is assumed to be negligible the turbulent displacement speed and the turbulent consumption speed are assumed to be equal. In order to obtain a more precise estimate of the consumption flame speed the flame thickness must be evaluated. This can be done by providing better estimates of the burned gas mass. The mass must include not only the fully burned gases but also the burned gases within the flame front itself. Poinsot and Veynante [20]

provide an expression for the consumption flame speed as a function of $r(t)$ which includes the effects of finite flame thickness. For a turbulent flame the consumption speed is defined as follows:

$$S_T^c = \left(1 + \frac{1}{2}\frac{\delta_L}{r(t)}(1 + \frac{\rho_u}{\rho_b})\right)\frac{\rho_b}{\rho_u}\frac{d}{dt}r(t) \tag{29}$$

As specified in Table 5 for flame ***F13***, $\delta_L = 56.01\ \mu m$ and $\delta_L^b = 405.3\ \mu m$. In order to correctly represent the impact of the turbulent flame consumption speed, calculation of the flame thickness is required as a function of time. Particularly for turbulent flames, the flame thickness increases in time. The turbulent consumption speed evaluated using δ_L and a radial position of 10 *mm* is 0.59 m/s. This varies little from the Monte-Carlo predicted displacement speed of 0.58 *m/s*. The evaluation of consumption flame speeds at larger radial locations is usually neglected due to this fact. However, using the more precise modified laminar flame thickness, δ_L^b, the consumption flame speed increases significantly to a value of 0.67 *m/s*. Therefore, the evaluation of the consumption flame speed based upon δ_L^b should not be neglected as the consumption speed varies greatly from the displacement speed even at larger radial distances.

5.7 Effect of Turbulence Intensity

The radial position of the flame as a function of time from spark onset is shown in Figure 10 for seven flames with increasing values of turbulence intensity. The flames represented are ***F2***, ***F3,*** ***F4***, ***F5***, ***F6***, ***F7*** and ***F8*** for ϕ = 0.8. The turbulence intensity ranges from 1.3 m/s to 1.6 *m/s*. The chemical and spark ignition conditions are identical in each of these seven flames. The only

variation occurred in the turbulent flow properties by increasing the turbulence intensity. The dissipation of the turbulent kinetic energy increased with each increase in the turbulence intensity in order to maintain a constant turbulence time of 2 *ms* in each flame simulation. Other properties associated with these flames are specified in table 5. It is observed that within the range of specified turbulence intensity values the turbulent absolute flame speed, S_T^a, and the turbulent displacement flame speed, S_T^d, increases with u'. Initially, for approximately 2 *ms*, there exists little variation in flame propagation among the seven flames. The flame does not display any sensitivity to the value of the turbulence intensity and travels at approximately the value of the laminar flame speed for ϕ = 0.8. At times greater than 2 *ms* flames ***F2-F8*** experience increasing rates of flame propagation. Turbulence convects, wrinkles, and stretches the flame sheet, increasing the flame area and thus the flame speed.

6 Conclusions

The effect of turbulence on a propagating premixed flame is a subject of long standing practical importance and continuing research**.** Incorporation of all influences into an ignition model and the use of appropriate turbulence models are essential for correct treatment of flame kernel formation. The present model considered several vital influences such as spark ignition energy losses, flow field effects, mixture properties and thermodynamic conditions upon early flame propagation. Emphasis is placed on the determination of various turbulent flame speeds including the absolute, displacement and consumption flame speed.

The model predicts a minimum ignition energy, $S_{ign\text{-}min}$, of approximately 0.3 *mJ* for ϕ = 0.9. This agrees well with the experimental values of 0.28 *mJ* cited by Lewis and Von Elbe [14]

and Glassman [9]. The model predicts a quenching distance of 2 *mm* that also matches the value observed by Lewis and Von Elbe [14].

For a turbulence intensity of $u' = 1.93$ *m/s* the predicted flame ball position matches very closely to the experimental values predicted by Hainsworth [13] and the numerical calculations of Pope and Cheng [22]. The present model demonstrates that during early ignition the flame travels at the laminar burning velocity for approximately 2 *ms* then increases to an asymptotic turbulent flame speed value. The asymptotic turbulent flame speed computed for $\phi = 0.8$ is 0.58 *m/s*.

The results verify an increase in flame propagation speed with increasing initial turbulence intensity. It is shown that even for varying turbulence intensities the duration of the initial phase of the flame that travels at S_L occurs for a period of approximately 2 *ms*. The present model predicts that increasing the turbulence intensity increases S_T and that the duration of the initial laminar portion of turbulent flames is affected very little by variation of the turbulence intensity.

Physically, the current model predicts the mean gas velocity to be highest inside the flame brush. There is significant radial motion of gases inside and well ahead of the flame in the unburned gas region. It is observed that the turbulent flame brush thickness increases with increasing time from ignition.

Calculation of the turbulent consumption speed based upon a modified laminar flame thickness provides a value of 0.67 *m/s*. This varies from the corresponding displacement speed by 15.5 percent and emphasizes the importance of the consumption flame speed. The effects of preferential diffusion cause the unburned-to-burned gas density ratio to vary as a function of flame stretch. However, it is difficult to calculate the variation of the density ratio across the flame front. Therefore, in the present analysis, a single density ratio was calculated using the

CEC Gordon McBride code [11]. Also, for fuel-lean conditions the effects of stretch are not as great as for fuel-rich conditions and, presumably, the density ratio does not vary significantly. This approach can be easily converted to correct the calculated burning velocities or displacement speeds once density ratios can be generated from well-established flame structure models. The theoretical treatment of flames in the distributed reaction zone was not handled differently than flames within the wrinkled or corrugated flame regimes. The Monte-Carlo results for various flames supports the latest views that flames in the distributed reaction zone regime are not as vulnerable to flame quenching as commonly believed. The distributed reaction zone regime has traditionally been viewed as incapable of sustaining a flame due to the fluctuations in temperature, concentration and velocity.

References

[1] Anand, M.S., and Pope, S.B. (1987). Calculations of Premixed Turbulent Flames by PDF Methods. *Combustion and Flame*, Vol. 67, pp. 127-142.

[2] Aung, K.T., Hassan, M.I. and Faeth, G.M. (1997). Flame Stretch Interactions of Laminar Premixed Hydrogen/Air Flames at Normal Temperature and Pressure. *Combustion and Flame,* Vol. 109, pp. 1-24.

[3] Blanc, M.V., Guest, P.G., Von Elbe, G., and Lewis, B. (1949). *Third Symposium (International) on Combustion/The Combustion Institute*, pp. 363.

[4] Borghi, R., and Mantel, T. (1994). A New Model of Premixed Wrinkled Flame Propagation Based on a Scalar Dissipation Equation. *Combustion and Flame.* Vol. 96, no. 4, pp. 443-457.

[5] Carmen, C.L. and Feikema, D.A. (1999). Monte-Carlo computation of turbulent premixed methane-air ignition. *Combustion, Explosion, and Shock Waves,* Vol. 34, no. 3, pp. 253-259.

[6] Carmen, C.L. (2003).Monte-Carlo Computation of Turbulent Premixed Methane/Air Ignition, Ph.D. Dissertation, University of Alabama in Huntsville.

[7] Cheng, R. K., Shepard, I. G., Bedat, B. and Talbot, L. (2002). Premixed Turbulent Flame Structures in Moderate and Intense Isotropic Turbulence. *Combust. Sci. and Tech.* Vol. 174, pp. 29-60.

[8] Curl, R.L. (1963). Dispersed Phase Mixing: I. Theory and Effects in Simple Reactors. *A.I.Ch.E. Journal,* Vol. 9, No. 2, pp.175-181.

[9] Dopazo, C. (1994). *Turbulent Reacting Flows*. ed Libby, P.A. and Williams, F.A. (London: Academic) pp. 375-474.

[10] Glassman, I. (1996). Combustion, Academic Press, San Diego, CA.

[11] Gordon, S., and McBride, G.J. (1971). Computer program for calculations of complex chemical equilibrium compositions, rocket performance, incident and reflected shocks, and chapman-jouguet detonations. *NASA Report* SP-273, Washington.

[12] Gülder, O.L. (1990). Turbulent premixed flame propagation models for different combustion regimes. *Twenty-Third Symposium (International) on Combustion/The Combustion Institute*, pp. 743-650.

[13] Gülder, O.L. (1990). Turbulent premixed combustion modeling using fractal geometry. *Twenty-Third Symposium (International) on Combustion/The Combustion Institute*, pp. 835-842.

[14] Hainsworth, E. (1985). Study of free turbulent premixed flames. M.S. Thesis, M.I.T.

[15] Lewis, B., and von Elbe, G. (1987). Combustion, Flames and Explosions of Gases, Fig. 171, Third Edition, Publishers Academic Press, Inc..

[16] Ma, J. X., Alexander, D. R., and Poulain, D. E. (1998). Laser Spark Ignition and Combustion Characteristics of Methane-Air Mixtures. *Combustion and Flame,* Vol. 112, pp. 492-506.

[17] Peters, N. (2000). Turbulent Combustion. Cambridge University Press.

[18] Poinsot, T.J. (1991). Flame ignition in a premixed turbulent flow. Center for Turbulence Research, Stanford University, Annual Research Briefs.

[19] Poinsot, T.J. (1998). Comments on Flame Stretch Interactions of Laminar Premixed Hydrogen Air Flames at Normal Temperature and Pressure by Aung et al. *Combustion and Flame.* Vol. 113, pp. 279-284.

[20] Poinsot, T.J. and Veynante, D. (2001). Theoretical and Numerical Combustion. R.T. Edwards, Inc.

[21] Pope, S. B. (1985). PDF Methods for Turbulent Reactive Flows. *Prog. Energy Combust. Sci.* Vol. 11, pp. 119-192.

[22] Pope, S. B. (1990). Computations of turbulent combustion: progress and challenges. In *Twenty-Third Symp. (Int.) on Combustion,* pp. 591-612. Pittsburgh: The Combustion Institute.

[23] Pope, S. B., and Cheng, W.K. (1986). Statistical calculations of spherical turbulent flames. *Twenty-first Symposium (International on Combustion/The Combustion Institute*, pp. 1473-1482.

[24] Rutland, C.J., Ferziger, J.H., and El Tahry, S.H. (1990). Full numerical simulations and modeling of turbulent premixed flames. *Twenty-third Symposium (International) on Combustion/The Combustion Institute*, pp. 621-627.

[25] Williams, F.A. (1985). Combustion Theory, Benjamin Cummings, Menlo Park, CA.

[26] Xu, J. and Pope, S. B. (1999). Numerical studies of PDF/Monte Carlo methods for turbulent reactive flows, *J. Comput. Phys*. Vol. 152, pp. 192-230.

[27] Zeldovich, Ya. B. (1941). *Zh. Eksp. Teor. Fiz.* 11, 159. See Shchetinkov, Ye. S. (1969). The Physics of the Combustion of Gases. Chapter 5, Edited Translation FTD-HT-23-496-68, Translation Revision, Foreign Technology Division, Wright-Patterson AFB, Ohio.

Figure Captions:

Figure 1.—Schematic of Spark-Ignited turbulent flame ball and Kinematic Balance between the Flame Propagation Velocity, Flow Velocity and Turbulent Burning Velocity.

Figure 2.—Ten Realizations and Average of the radial flame propagation as defined by flame position as a function of time. Initial flame properties: Premixed Methane/Air mixture, $\phi = 0.8$, u' = 0.7 m/s, Initially Gaussian Distribution for velocity with U = 0.0 m/s. Initially 100 particles distributed per cell.

Figure 3.—Ten Realizations and Average of the radial flame propagation as defined by flame position as a function of time. Initial flame properties: Premixed Methane/Air mixture, $\phi = 0.8$, u' = 0.7 m/s, Initially Gaussian Distribution for velocity with U = 0.0 m/s. Initially 1000 particles distributed per cell.

Figure 4.—Borghi-Barrière Regime diagram for turbulent premixed flames.

Figure 5.—Time evolution of the normalized fuel concentration as a function of radial position for flame F1. Initial flame properties: Premixed Methane/Air mixture, $\phi = 0.8$, u' = 0.7 m/s, Initially Gaussian Distribution for velocity with U = 0.0 m/s. Initially 1000 particles distributed per cell.

Figure 6.—Time evolution of the cell averaged gas density as a function of radial position for flame F1. Initial flame properties: Premixed Methane/Air mixture, $\phi = 0.8$, u' = 0.7 m/s, Initially Gaussian Distribution for velocity with U = 0.0 m/s. Initially 1000 particles distributed per cell.

Figure 7.—Time evolution of the cell averaged mean gas velocity as a function of radial position for flame F1. Initial flame properties: Premixed Methane/Air mixture, $\phi = 0.8$, u' = 0.7 m/s, Initially Gaussian Distribution for velocity with U = 0.0 m/s. Initially 1000 particles distributed per cell.

Figure 8.—Three Dimensional Time evolution of the cell averaged mean gas velocity as a function of radial position and time from spark onset for flame F1. Initial flame properties: Premixed Methane/Air mixture, $\phi = 0.8$, u' = 0.7 m/s, Initially Gaussian Distribution for velocity with U = 0.0 m/s. Initially 1000 particles distributed per cell.

Figure 9.—Comparison of the flame propagation as defined by flame position as a function of time for flame F13. Initial flame properties: Premixed Methane/Air mixture, $\phi = 0.8$, u' = 1.93 m/s, Initially Gaussian Distribution for velocity with U = 0.0 m/s. Initially 1000 particles distributed per cell.

Figure 10.—Effect of turbulence intensity on the flame propagation as defined by flame position as a function of time for flames F2, F3, F4, F5, F6, F7, and F8. Initial flame properties: Premixed Methane/Air mixture, $\phi = 0.8$, u' = 1.3 to 1.6 m/s, Initially Gaussian Distribution for velocity with U = 0.0 m/s. Initially 1000 particles distributed per cell.

Table 5

Flame	ϕ	Re_T	Da_T	k (m^2/s^2)	u' (m/s)	S_L (m/s)	S_L^d (m/s)	$\frac{u'}{S_L}$	$\frac{u'}{S_L^d}$	ε (m^2/s^3)	δ_L (μm)	δ_L^b (μm)	l_T (mm)	λ (μm)	η (μm)	t_{chem} (ms)	t_T (ms)	t_η (ms)	Ka'	Ka	t_{sp} (ms)	L_{sp} (mm)	S_{ign} (mJ)
F1	0.8	62	10.	.735	0.7	0.28	.28	2.5	2.5	245	56.08	405.9	1.4	177.80	63.9	0.2	2.0	0.253	1.08	.791	1.5	2.5	1.5
F2	0.8	244	10.	2.535	1.3	0.28	.28	2.5	2.5	745	56.13	406.2	2.95	188.85	47.7	0.2	2.0	0.145	1.38	1.40	2.5	2.5	2.1
F3	0.8	232	10.	2.734	1.35	0.28	.28	2.5	2.5	911	56.11	406.1	2.7	177.26	45.4	0.2	2.0	0.131	1.53	1.53	2.5	2.5	2.1
F4	0.8	250	10.	2.94	1.4	0.28	.28	2.5	2.5	980	56.00	405.3	2.8	177.09	44.6	0.2	2.0	0.127	1.58	1.57	2.5	2.5	2.1
F5	0.8	268	10.	3.15	1.45	0.28	.28	2.5	2.5	1050	56.04	405.6	2.9	177.15	43.8	0.2	2.0	0.122	1.64	1.64	2.5	2.5	2.1
F6	0.8	287	10.	3.375	1.5	0.28	.28	2.5	2.5	1125	56.00	405.3	3.0	177.08	43.1	0.2	2.0	0.118	1.69	1.69	2.5	2.5	2.1
F7	0.8	306	10.	3.6	1.55	0.28	.28	2.5	2.5	1200	56.08	405.9	3.1	177.22	42.4	0.2	2.0	0.114	1.75	1.75	2.5	2.5	2.1
F8	0.8	326	10.	3.84	1.6	0.28	.28	2.5	2.5	1280	56.09	405.9	3.2	177.23	41.7	0.2	2.0	0.111	1.81	1.80	2.5	2.5	2.1
F9	0.8	368	10.	4.335	1.7	0.28	.28	2.5	2.5	1445	56.09	405.9	3.4	177.24	40.5	0.2	2.0	0.104	1.92	1.92	2.5	2.5	2.1
F10	0.8	389	10.	4.59	1.75	0.28	.28	2.5	2.5	1531	56.23	406.9	3.5	177.45	39.9	0.2	2.0	0.101	1.98	1.98	2.5	2.5	2.1
F11	0.8	413	10.	4.86	1.8	0.28	.28	2.5	2.5	1620	56.04	405.6	3.6	177.14	39.3	0.2	2.0	0.098	2.03	2.04	2.5	2.5	2.1
F12	0.8	460	10.	5.415	1.9	0.28	.28	2.5	2.5	1805	56.06	405.7	3.8	177.18	38.3	0.2	2.0	0.093	2.15	2.15	2.5	2.5	2.1
F13	0.8	475	10.	5.59	1.93	0.28	.28	2.5	2.5	1862	56.01	405.3	3.86	177.11	38.0	0.2	2.0	0.092	2.18	2.17	2.5	2.5	2.1
F14	0.8	508	10.	6.0	2.0	0.28	.28	2.5	2.5	2000.	56.10	406.0	3.99	177.03	37.3	0.2	2.0	0.089	2.26	2.25	2.5	2.5	2.1
F15	0.8	617	10.	7.26	2.2	0.28	.28	2.5	2.5	2420.	56.03	405.5	4.4	177.13	35.6	0.2	2.0	0.081	2.49	2.47	2.5	2.5	2.1

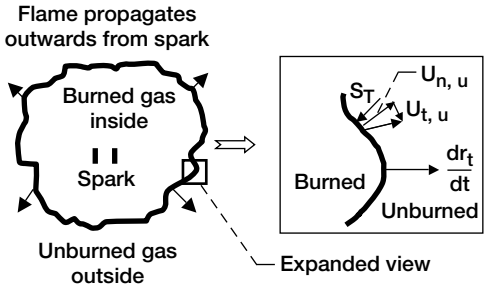
Flame propagates
outwards from spark
Burned gas
inside
Spark
Unburned gas
outside
S_T
$U_{n,\,u}$
$U_{t,\,u}$
$\frac{dr_t}{dt}$
Burned
Unburned
Expanded view

Figure 1.

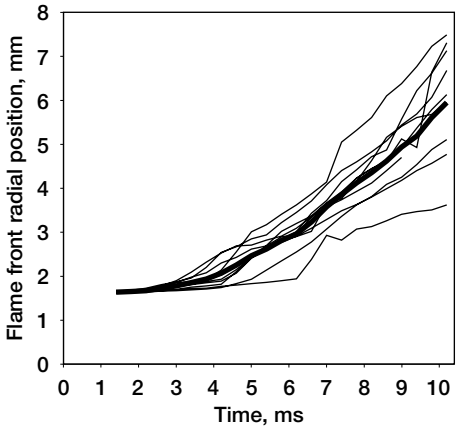
Flame front radial position, mm
0
1
2
3
4
5
6
7
8
0 1 2 3 4 5 6 7 8 9 10
Time, ms

Figure 2.

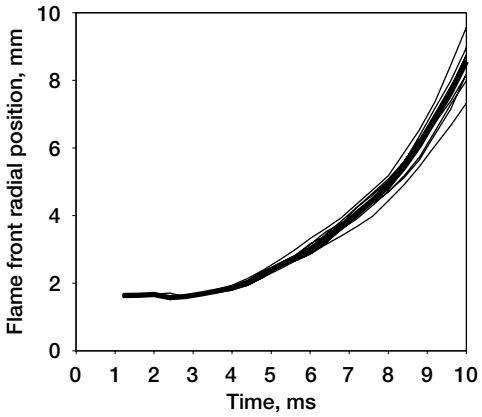
Flame front radial position, mm
0
2
4
6
8
10
0 1 2 3 4 5 6 7 8 9 10
Time, ms

Figure 3.

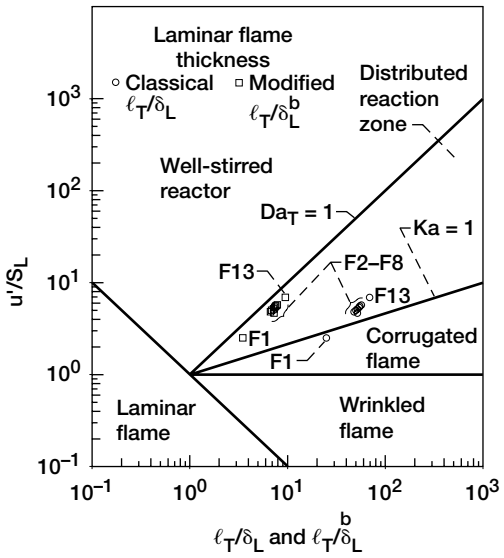
Laminar flame thickness
Classical ℓ_T/δ_L
Modified ℓ_T/δ_L^b
Distributed reaction zone
Well-stirred reactor
$Da_T = 1$
Ka = 1
F13
F2–F8
F13
F1
F1
Corrugated flame
Laminar flame
Wrinkled flame
u'/S_L
10^3
10^2
10^1
10^0
10^{-1}
10^{-1}
10^0
10^1
10^2
10^3
ℓ_T/δ_L and ℓ_T/δ_L^b

Figure 4.

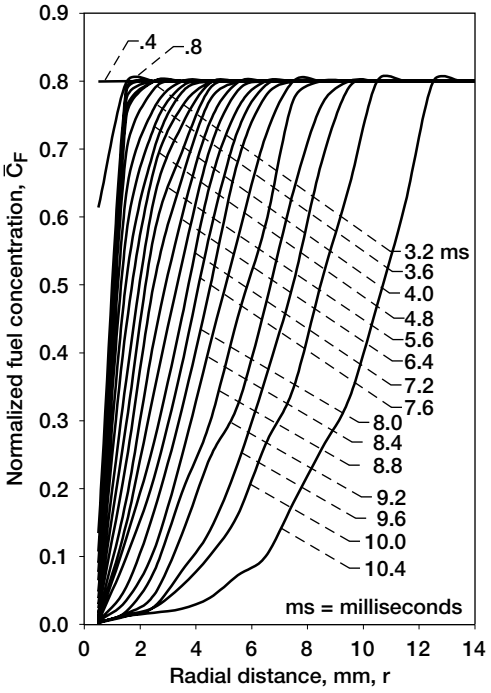
0.9
0.8
0.7
0.6
0.5
0.4
0.3
0.2
0.1
0.0
Normalized fuel concentration, $\bar{C}_F$
.4
.8
3.2 ms
3.6
4.0
4.8
5.6
6.4
7.2
7.6
8.0
8.4
8.8
9.2
9.6
10.0
10.4
ms = milliseconds
0
2
4
6
8
10
12
14
Radial distance, mm, r

Figure 5.

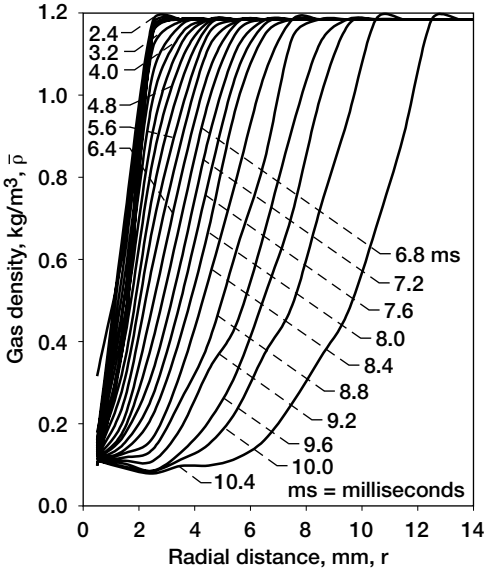
1.2
1.0
0.8
0.6
0.4
0.2
0.0
Gas density, kg/m3, ρ̄
0
2
4
6
8
10
12
14
Radial distance, mm, r
2.4
3.2
4.0
4.8
5.6
6.4
6.8 ms
7.2
7.6
8.0
8.4
8.8
9.2
9.6
10.0
10.4
ms = milliseconds

Figure 6.

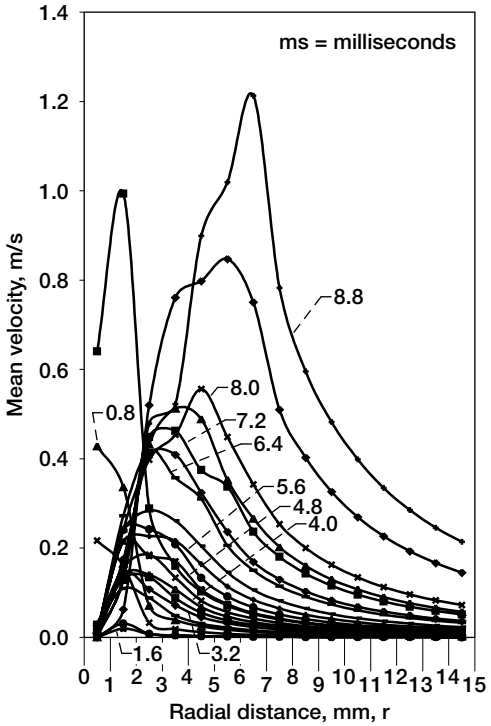
ms = milliseconds
Mean velocity, m/s
Radial distance, mm, r
0.8
1.6
3.2
4.0
4.8
5.6
6.4
7.2
8.0
8.8

Figure 7.

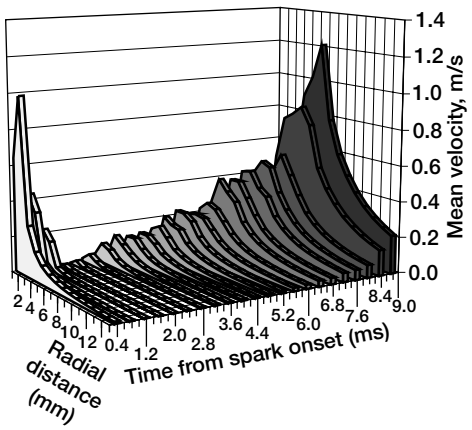
1.4
1.2
1.0
0.8
0.6
0.4
0.2
0.0
Mean velocity, m/s
2 4 6 8 10 12
Radial distance (mm)
0.4 1.2 2.0 2.8 3.6 4.4 5.2 6.0 6.8 7.6 8.4 9.0
Time from spark onset (ms)

Figure 8.

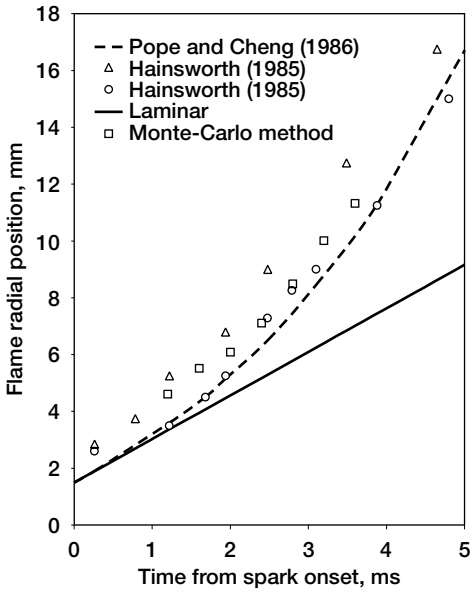
Pope and Cheng (1986)
Hainsworth (1985)
Hainsworth (1985)
Laminar
Monte-Carlo method
Flame radial position, mm
Time from spark onset, ms
0
2
4
6
8
10
12
14
16
18
0
1
2
3
4
5

Figure 9.

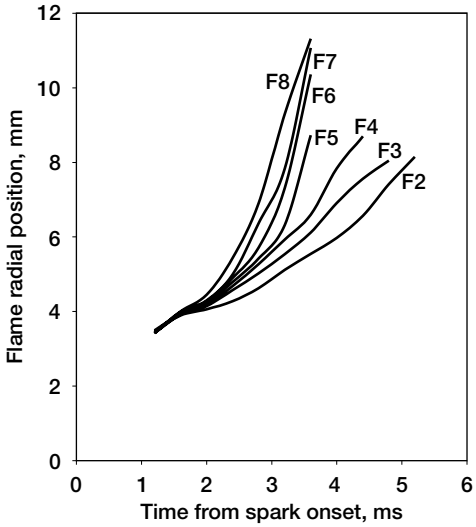
Flame radial position, mm
Time from spark onset, ms
F8
F7
F6
F5
F4
F3
F2
0
2
4
6
8
10
12
0
1
2
3
4
5
6

Figure 10.